Clays and Clay Minerals, Vol. 67, No. 1:25–43, 2019

VECTORIZED CLAY NANOPARTICLES IN THERAPY AND DIAGNOSIS

Goeun Choi[1,2], Huiyan Piao[1], Sairan Eom[1], and Jin-Ho Choy[1,*]

[1]Center for Intelligent Nano-Bio Materials (CINBM), Department of Chemistry and Nanoscience, Ewha Womans University, Seoul 03760, Republic of Korea

[2]Institute of Tissue Regeneration Engineering (ITREN), Dankook University, Cheonan 31116, Republic of Korea

Abstract—Over the past several decades, clay minerals have been applied in various bio-fields such as drug and drug additives, animal medicine and feed additives, cosmetics, biosensors, etc. Among various research areas, however, the medical application of clay minerals is an emerging field not only in academia but also in industry. In particular, cationic and anionic clays have long been considered as drug delivery vehicles for developing advanced drug delivery systems (DDSs), which is the most important of the various research fields including new drugs and medicines, in vitro and in vivo diagnostics, implants, biocompatible materials, etc., in nanomedicine. These applications are obviously related to global issues such as improvements in welfare and quality of life with life expectancy increasing. Many scientists, therefore, in various disciplines, such as clay mineralogy, material chemistry, molecular biology, pharmacology, and medical science, have been endeavoring to find solutions to such global issues. One of the strategic approaches is probably to explore new drugs possessing intrinsic therapeutic effects or to develop advanced materials with theranostic functions. With this is mind, discussions of examples of cationic and anionic clays with bio- and medical applications based on nanomedicine are relevant. In this tutorial review, nanomedicine based on clay minerals are described in terms of synthetic strategies of clay nanohybrids, in vitro and in vivo toxicity, biocompatibility, oral and injectable medications, diagnostics, theranosis, etc.

Keywords—Anionic Clay · Biocompatibility · Cationic Clay · Diagnostics · Drug Delivery · Inorganic Nanovehicle · Layered Double Hydroxides · Medicinal Application · Toxicity

INTRODUCTION

Much attention has been paid in recent years to the medicinal applications of clay minerals due to their abundance in nature and unlimited potential (Reichle, 1986; Choy, 2004). Clay minerals have been used especially for different biological applications including biocompatible materials, biosensors, pharmaceuticals, cosmetics, and nanomedicine (Choy et al. 1999; Choy et al. 2000; Choi et al. 2018). This is surely due to their excellent physicochemical and biological properties, such as large surface area, large ion exchange capacity, intercalative swelling behavior, excellent biocompatibility, and low toxicity (Baek et al. 2012; Gaharwar et al., 2013; Xavier et al., 2015).

Clay minerals can be classified into neutral, cationic, and anionic clays with respect to their layer charge (Table 1). A wide variety of clay minerals such as halloysite, montmorillonite (Mnt), Laponite®, layered double hydroxide (LDH), layered double salt (LDS), and others have been studied extensively as vectorized clays, namely, advanced drug delivery vehicles for their potential biomedical applications.

In this review, the key aspects of clay chemistry will be discussed with a specific focus on the nanomedical applications of cationic and anionic clay minerals, and their nanohybrids formed with drugs or bioactive molecules.

Cationic clay

Cationic clays are phyllosilicates comprising tetrahedral silicate sheets and octahedral Mg or Al oxyhydroxide sheets (Fig. 1A). They are divided into two main classes: 1:1 and 2:1 types (Fig. 1A,B), depending on their arrangements of octahedral and tetrahedral sheets along the crystallographic *c* axis. As for the 1:1 type clay (e.g. kaolinite and halloysite) with the unit-cell formula of $Al_2Si_2O_5(OH)_4$, each layer is electrically neutral, and its interlayer interaction is of a molecular nature such as hydrogen bonding or van der Waals force (Bergaya & Lagaly, 2006). One thing to note here is that the 1:1 type clay minerals, in general, have very small cation exchange capacities (CEC) compared with 2:1 type clay minerals. Unlike kaolinite, halloysite layers are hydrated and rolled up into nanotubes giving rise to larger specific surface areas (SSA) with different internal and external surface properties (Yuan et al. 2015). Such an unusual porous structure enables halloysite nanotubes to be drug delivery vectors in nanomedicine (Lvov et al. 2016). For the 2:1 type clays with the unit-cell formula of $M_xSi_4O_{10}(OH)_2$ (e.g. mica, chlorite, vermiculite, and montmorillonite), each layer consists of an octahedral sheet sandwiched between two tetrahedral ones, where M_x is Al_2^{3+} for the dioctahedral clay, and M_x is Mg_3^{2+} for the trioctahedral sheet. If the octahedral and/or tetrahedral metal ions were substituted by cations with smaller valencies, a negative layer charge could be developed. In order to balance this layer charge and its distribution, cations are stabilized in the interlayer space of a clay lattice and in general solvated, which can, however, be replaced by other inorganic or organic cations by a simple ion-exchange reaction depending on the CEC values of the 2:1 type clays. Negatively charged drugs or bioactive molecules, therefore, have been encapsulated in the interlayer space of the clay for exploring advanced drug delivery systems based on clays.

Anionic clay

Layered double hydroxides (LDH) belong to a class of anionic clays. Unlike cationic clays, individual cationic brucite-like layers are stacked on top of each other with exchangeable anions in the interlayer space (along with water molecules) (Fig. 2a). The general formula of LDH can be expressed as $[M(II)_{1-x}M(III)_x(OH)_2][A^{m-}]_{x/m}\cdot nH_2O$, where M(II) is a divalent cation (Mg^{2+}, Ca^{2+}, Zn^{2+}, Co^{2+}, Cu^{2+}, Ni^{2+},

* E-mail address of corresponding author: jhchoy@ewha.ac.kr
DOI: 10.1007/s42860-019-0009-9

https://doi.org/10.1007/s42860-019-0009-9 Published online by Cambridge University Press

Table 1 Bio-applications of clay minerals

Species	General chemical formula	Application	Reference
Kaolinite	$Al_2Si_2O_5(OH)_4$	Hemostasis	Long et al. (2018)
		Bone tissue engineering	Wang et al. (2014)
Halloysite	$Al_2Si_2O_5(OH)_4 \cdot nH_2O$	Chemotherapy	Wen et al. (2015)
		Chemotherapy	Massaro et al. (2015)
		Anti-bacterial	Wei et al. (2014)
		Anti-oxidant	Vergaro et al. (2010)
		Cosmetics	Stockert et al. (2012)
Montmorillonite (Mnt)	$(Na,Ca)_{0.3}(Al,Mg)_2Si_4O_{10}(OH)_2 \cdot nH_2O$	Biosensor	Ding et al. (2016)
		Anti-bacterial	Saha et al. (2014)
		Oral drug delivery	Yang et al. (2007)
		Oral gene delivery	Kawase et al. (2004)
		Taste masking	Lee et al. (2012)
		Controlled release	Park et al. (2013)
Laponite®	$Na_{0.7}Si_8Mg_{5.5}Li_{0.3}O_{20}(OH)_4$	Chemotherapy	Zhou et al. (2016)
		In vivo MR imaging	Demir et al. (2014)
		Bone tissue engineering	Nair et al. (2016)
		In vivo CT imaging	Mustafa et al. (2016)
		Biosensor	Joshi et al. (2015)
		Anti-bacterial	Hamilton et al. (2014)
		Wound healing	Ghadiri et al. (2014)
Layered double hydroxide (LDH)	$[M(II)_{1-x}M(III)_x(OH)_2][A^{m-}]_{x/m} \cdot nH_2O$	Boron neutron capture therapy	Choi et al. (2017)
		Bone regeneration	Kim et al. (2014)
		Gene delivery	Park et al. (2016)
		Chemotherapy	Choi et al. (2012)
		Bio imaging	Kim, Lee, et al. (2016)
		In vivo CT/MR imaging	Wang et al. (2014)
		Anti-bacterial	Ryu et al. (2010)
Layered double salt (LDS)	$M^{2+}(OH)_{2-x}(A^{m-})_{x/m} \cdot nH_2O$	Oral drug delivery	Kim et al. (2016)
		Drug delivery	Bull et al. (2011)
		Anti-oxidant	Biswick et al. (2009)
		Controlled release	Yang et al. (2014)
Hydrocalumite	$[Ca_2M(OH)_6]^+A^- \cdot nH_2O$	Biosensor	Suh et al. (2011)
		Oral calcium supplement	Kim et al. (2015)

etc.), M(III) is an isomorphously substituted trivalent cation (Al^{3+}, Fe^{3+}, Co^{3+}, Ga^{3+}, etc.), and A^{m-} is an interlayer anion with charge m (Cl^-, NO_3^-, CO_3^-, SO_4^{2-}, etc.). Various kinds of inorganic or organic anions have been introduced between the hydroxide layers by simple anion exchange reaction or co-precipitation reaction (Choy et al., 1999). Layered double salt (LDS) is a family of LDH, and very similar in terms of crystal structure, which consists of positively charged layers and charge-compensating anions along the crystallographic c axis, but different in its layer composition (Kaassis et al., 2016; Bull et al. 2011). In the LDS structure, however, only divalent metal cations are octahedrally coordinated with hydroxo ligands to form hydroxide layers, and its general formula can be described as $M^{2+}(OH)_{2-x}(A^{m-}{}_{x/m} \cdot nH_2O$, where M is a divalent cation (Zn^{2+}, Co^{2+}, Cu^{2+}, Ni^{2+}, etc.), and A^{m-} is an anion with charge m (Cl^-, NO_3^-, CO_3^{2-}, SO_4^{2-},etc.). For example, Zn-containing LDS is known as the zinc basic salt (ZBS) with a chemical formula $[Zn_5(OH)_8](NO_3)_2 \cdot nH_2O$ (Fig. 2B). The crystal structure of ZBS comprises edge-sharing $Zn(OH)_6$ octahedra, and tetrahedrally coordinated $Zn(OH)_4$ units, which are formed on the upper and lower sides of vacant octahedral sites. Those units, therefore, are exposed to the internal surface of ZBS layers and further ligated with water molecules (Yang et al., 2007; Kim et al., 2015). Such a ZBS has been known as a family of 2D compounds structurally well defined and chemically stable, and, therefore, studied extensively as biomolecular reservoirs or advanced drug delivery systems (Oh et al., 2009).

Hydrocalumite belongs to LDHs in a broad sense, and its general formula can be expressed as $[Ca_2M(OH)_6]^+A^- \cdot nH_2O$. From the crystal structure point of view, hydrocalumite is similar to LDHs, as it also consists of self-assembled

https://doi.org/10.1007/s42860-019-0009-9 Published online by Cambridge University Press

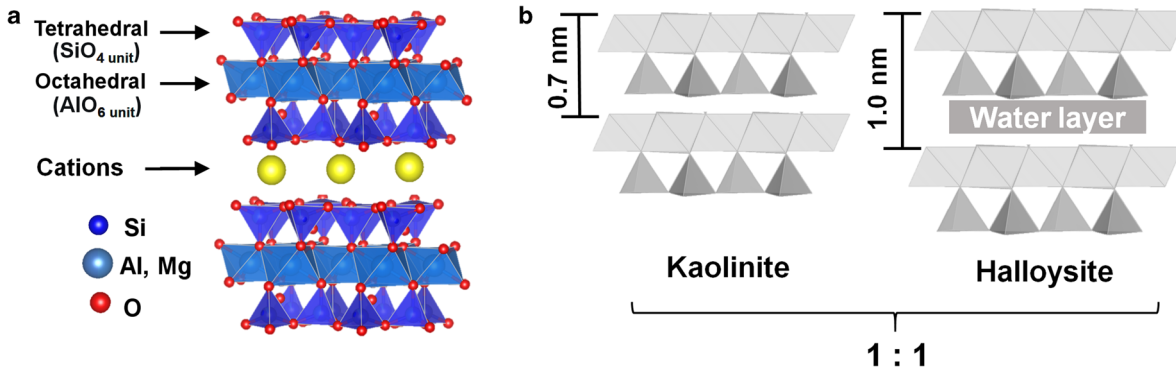

Fig. 1 Schematic crystal structures for **a** 2:1 type, and **b** 1:1 type clay minerals along the *c* axis

$(Ca(OH)_2)$ layers where Ca^{2+} ions are replaced partially by M^{3+} (Al^{3+} or Fe^{3+}) ions and in such a way a positive layer charge can be generated. As a result, incorporation of interlayer anions, such as CO_3^{2-}, Cl^-, and OH^-, are required to balance the resulting positive layer charge (Wen et al. 2015) (Fig. 2c). Obviously, hydrocalumites have some common characteristics with LDHs (Kim et al. 2014).

TOXICITY AND BIOCOMPATIBILITY

In vitro

Various cell lines have been used to study the toxicities induced by clays and clay-containing nanocomposites (Maisanaba et al., 2015). In the case of in vitro toxicological evaluation based on a colorimetric assay using the tetrazolium salt thiazolyl blue, the MTT assay after **m**ethyl-**t**hiazolyl-**t**etrazolium (Mosmann, 1983) has been applied widely for estimating cytotoxicity, cell viability, and proliferation. The MTT agent yields a yellowish solution, but results in violet-blue formazan crystals upon reduction by dehydrogenases present in metabolically active cells (Fig. 3). The lipid soluble formazan product can be extracted using organic solvents and evaluated by spectrophotometry (Stockert, Blázquez-Castro, Cañete, Horobin, & Villanueva, 2012). A 2:1 type clay such as montmorillonite (Mnt) inhibits significantly cell proliferation after 24–72 h incubation time and at concentration levels >100 μg/mL (Table 2; Baek et al., 2012). MgAl-LDH and ZnAl-LDH, the most frequently studied drug delivery

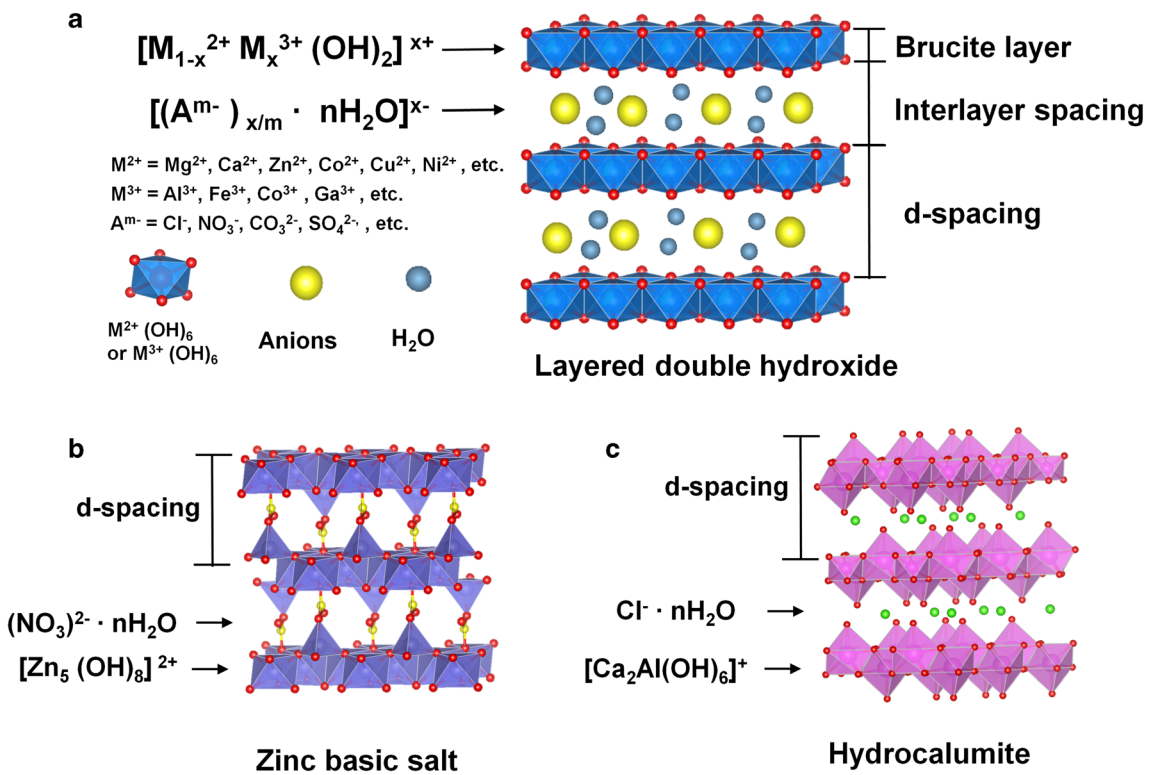

Fig. 2 Schematic crystal structures of **a** layered double hydroxide (LDH), **b** zinc basic salt (ZBS), and **c** hydrocalumite

https://doi.org/10.1007/s42860-019-0009-9 Published online by Cambridge University Press

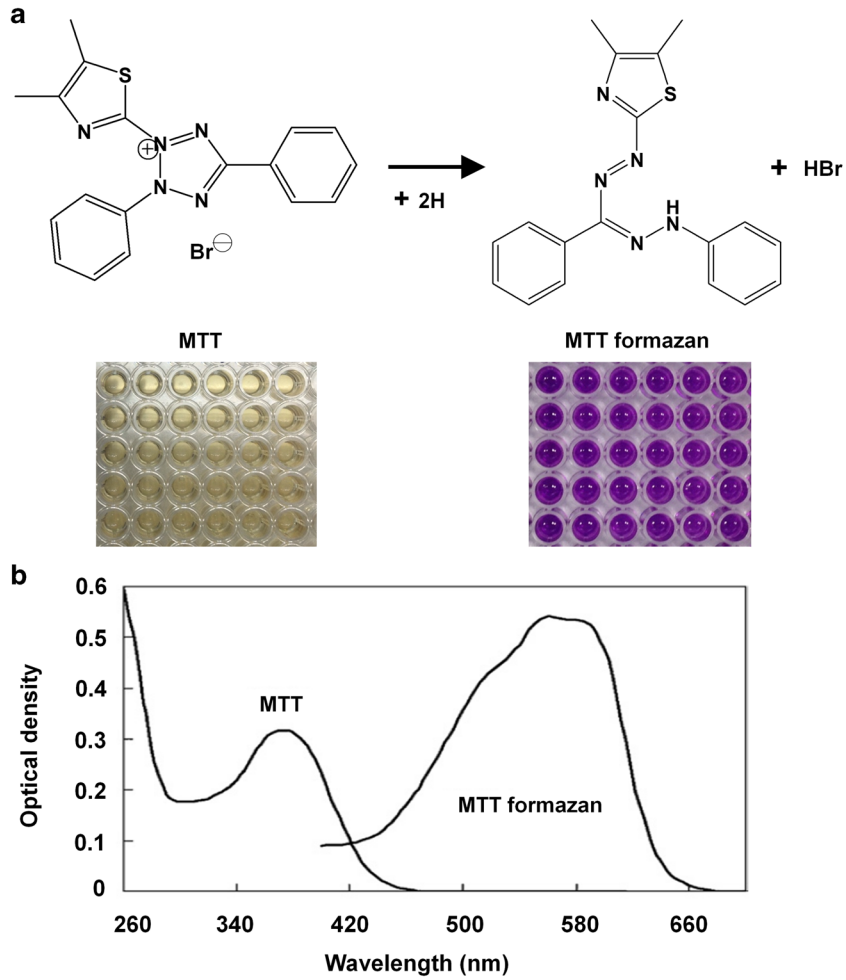

Fig. 3 (**a**) Chemical structures and colors of MTT and its reduced formazan product, and (**b**) absorption spectra of MTT and MTT formazan (after Stockert et al. 2012, reproduced with permission from Elsevier)

carriers, have been determined to be very low in toxicity at the concentration level of practical application as drug delivery systems. LDH clay at the nano-scale, therefore, has been suggested as an advanced drug delivery vector (Choi, Oh, Park, & Choy, 2007).

In vivo

According to bio-distribution studies of LDH nanoparticles in various organs (Fig. 4), the ionic concentrations of Mg and Al in LDH can be determined by inductively coupled plasma-atomic emission spectrometry (ICP-AES). In in vivo studies, tumors and various organs were harvested from each treatment group 1 day after the last injection, and then dissolved completely in an aqueous solution of HCl and H_2O_2. The Mg and Al ion concentrations were similar among the groups within the error limit for all the organs evaluated (Fig. 4). Surprisingly, LDH clay nanoparticles were not accumulated in tissue upon treatment with the MCF7/mot orthotropic breast-cancer mouse model (Choi, Kwon, Oh, Yun, & Choy, 2014).

Park et al. (2016) reported recently on in vivo safety of LDH as an anionic clay nanovehicle. No liver toxicity was observed up to a dosage of 125 mg/kg of LDH-FA(Folate)/siSurvivin corresponding to 2.5 mg/kg of siSurvivin (Fig. 5); the levels of inflammatory cytokine interleukin (IL)-6 (3.8 pg/mL), alanine transaminase (ALT) (57.7 pg/mL), and aspartate transaminase (AST) (109.6 pg/mL) were found to be in the normal ranges. Liver tissues were also studied using the hematoxylin and eosin (H&E) staining method, and found to be undamaged. The in vivo toxicity of FA-conjugated LDH (LDH-FA) nanocarrier was also tested in order to evaluate the therapeutic dosages and the toxicity of LDH-FA/siSurvivin. The LD_{50} (lethal dose 50%) value for LDH-FA was found to be >600 mg/kg, placing it in the non-toxic class.

DESIGN OF CLAY HYBRID SYSTEMS

Clay minerals have been designed as hybrid materials in order to optimize their characteristics for specific biological and medical applications. Because clay minerals have large surface areas, adsorption capacity, and ion exchange capacity, they can be hybridized easily with drugs, genes, bioactive molecules, biopolymers, and other functional organic molecules.

https://doi.org/10.1007/s42860-019-0009-9 Published online by Cambridge University Press

https://doi.org/10.1007/s42860-019-0009-9 Published online by Cambridge University Press

Table 2 In vitro and in vivo toxicities of clay minerals and their clay hybrids

	Species	Experimental methods	Results	Reference
In vitro	Montmorillonite (Mnt)	Effect of Mnt on cell proliferation of human normal intestinal (INT-407) cells after 24, 48, and 72 h	IC_{50} (inhibition concentration 50%) values; 565.50 μg/mL (24 h), 428.71 μg/mL (48 h), and 192.52 μg/mL (72 h)	Baek et al. (2012)
	Aminopropyl-functionalized magnesium (AMP) and calcium (ACP) organophyllosilicate	MTT assay of lung epithelial cancer (A549), lung fibroblast (MRC5), colon epithelial cancer (HT-29), and skin fibroblast (CCD986sk) cells	Little toxicity toward the proliferation or viability of cells	Han et al. (2011)
	Halloysite Nanotubes (HNTs)	MTT assay of cervical cancer (HeLa), and breast adenocarcinoma cells (MCF-7) cells	Non-toxic up to concentrations of 75 μg/mL	Vergaro et al. (2012)
	- $Mg_{0.68}Al_{0.32}(OH)_2(CO_3)_{0.16}{\cdot}0.1H_2O$; MgAl-LDH - $Zn_{0.68}Al_{0.32}(OH)_2(CO_3)_{0.16}{\cdot}0.1H_2O$; ZnAl-LDH	MTT assay of human normal lung (L-132), hepatoblastoma (HepG2), and breast adenocarcinoma cells (MCF-7) cells	Little toxicity toward the proliferation or viability of cells (~500 μg/mL)	Choi et al. (2016)
In vivo	Montmorillonite (Mnt)	Acute oral toxicity of Mnt; single dose administration of four different doses (5, 50, 300, and 1000 mg/kg) in mice	- The LD_{50} (lethal dose 50%) values were > 1000 mg/kg - No mortality was found in all the mice treated with different doses of Mnt.	Baek et al. (2012)
	Halloysite Nanotubes (HNTs)	- Biodistributions of Al and Si - Histopathological Test	Oral administration of HNTs significantly increased Al content but did not markedly affect Si content in the lung. This study provides the first evidence that oral HNTs at high dose could be absorbed from the gastrointestinal tract and deposited in the lung and could also induce pulmonary fibrosis.	Wang et al. (2013)
	$Mg_{0.68}Al_{0.32}(OH)_2\ (CO_3)_{0.16}{\cdot}0.1H_2O$; MgAl-LDH	Change in body weight in LDHs-administered mice for 4 weeks.	Different-sized LDHs did not cause any mortality or body weight loss up to 600 mg/kg.	Choi et al. (2007)

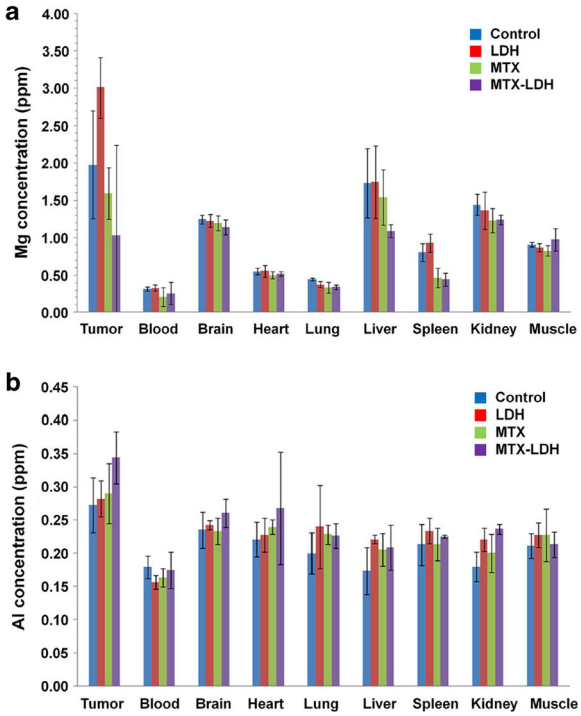

Fig. 4 (**a**) and (**b**) accumulation of LDH nanoparticles in organs of tumor-bearing mice treated with PBS (control), LDH, MTX, or MTX-LDH for 5 weeks ($n = 3$ for each group). On the first day after the final treatment, the mice were sacrificed and organs, blood, and tumors were collected for measurement of Mg and Al contents, the major components of LDH (after Choi et al. 2014, reproduced with the permission of Nature Research)

Modification of clay hybrid materials

Many studies of hybridization of clay minerals have been focused on the surface modification by surfactants and polymers. Prepared hybrid-clays can thus be utilized as the drug delivery systems with designed functions such as controlled drug release, targeted drug delivery, enhanced solubility, improved chemical stability, etc.

Lee et al. (2012), for example, intercalated a cationic drug (sildenafil) into the negatively charged Mnt layers through an ion-exchange reaction. To improve the taste-masking efficiency and enhance the rate of drug-release, the sildenafil-Mnt hybrids were further modified with AEA (polyvinylacetal diethylaminoacetate) (Fig. 6a). For oral medication, AEA is insoluble in the buccal cavity, but its release rate can be enhanced in gastric juice, due to the high solubility of AEA in acidic conditions.

Using a different approach, Wang et al. (2014) reported Laponite®-drug-polymer nanohybrids with enhanced cytocompatibility, pH-stimulative controlled release property, and physiological stability. In this case, a cationic drug (doxorubicin) was intercalated into Laponite® and then further modified with PEG-PLA (polyethylene glycol-polylacic acid) copolymer by a self-assembling method (Fig. 6b), but a biodistribution study is required to understand accumulation of the drug in various organs in the body.

Yang et al. (2014) also tried to intercalate telmisartan, an antihypertensive drug (poor water solubility), into 3-aminopropyl functionalized magnesium phyllosilicate (aminoclay) in order to improve the bioavailability of the drug for oral administration, because the surface charge of an aminoclay becomes positive due to the amine groups functionalized on clay. A positively charged aminoclay, therefore, can intercalate or adsorb negatively charged telmisartan via an electrostatic interaction resulting in the formation of a weakly coupled telmisartan-aminoclay complex, which showed an enhanced bioavailability of a poorly soluble drug (Fig. 6c).

Yah et al. (2012) studied functional halloysite by modifying its surface with various molecules, taking advantage of the inner-surface chemistry of halloysite nanotubes which is different from the outer-surface chemistry. Selective functionalization of the halloysite clay lumen resulted in a hydrophobic aliphatic chain core with micelle-like architecture and a hydrophilic silicate shell. The internal surface of halloysite was first modified with octadecylphosphonic acid (Fig. 6d), and then the external surface with silylating agent, *N*-(2-aminoethyl)-3-aminopropyltriethoxysilane, giving rise to a difference in chemical reactivity between the inner and outer surfaces of the clay nanotubes, and, therefore, the functionalized halloysite can be used for drug reservoir and delivery.

Synthetic method of clay hybrid materials

Despite the variety of clay minerals in nature, clay hybrid systems can be explored on the basis of a synthetic clay for medical applications. Several synthetic routes to anionic clay nanohybrid materials, such as co-precipitation, ion-exchange, exfoliation-reassembling, and calcination-reconstruction (Margarita et al. 2005; Park et al., 2013; Choi et al., 2018), have been studied extensively (Fig. 7).

The co-precipitation method is a simple and economic technique for the preparation of LDH hybrid materials, which can be achieved by base titration of a metal salt [M^{2+} and M^{3+} (or mixtures)] precursor solution in the presence of anionic drug or biofunctional molecules. In this way, anionic drug or guest molecules can be incorporated simultaneously into the LDH lattice to form LDH hybrid. To obtain LDH hybrid as a precipitate, the solution pH must be adjusted carefully to a coprecipitation range of corresponding metal hydroxides by considering the pCi [log(ionic concentration)] values with respect to pH and the pK_a values of functional groups in biomolecules. Based on this solution chemistry, a wide variety of biomolecules can be intercalated directly into an anionic clay lattice. To control the particle size and enhance the crystallinity of the clay, the hydrothermal method can be used selectively.

The ion exchange process is a classical way of preparing clay hybrid materials, where the negatively charged guest molecules in the solution can be exchanged with the anions present in the interlayer species of clays. The ion exchange reaction can, in general, be affected by some factors, such as the ion exchange capacity of LDH, the solution pH, and the thermodynamic stability between host LDH and guest molecules.

https://doi.org/10.1007/s42860-019-0009-9 Published online by Cambridge University Press

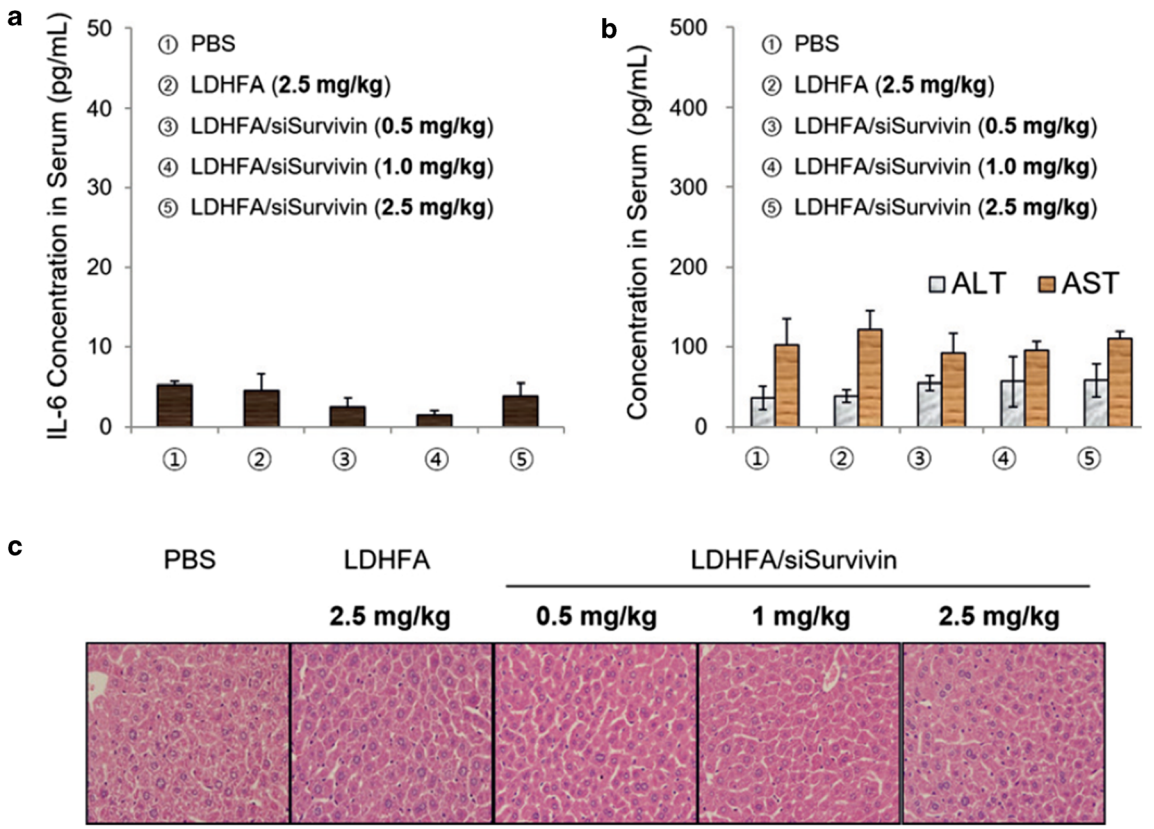

Fig. 5 Innate immune responses and liver toxicity of the LDH-FA/siSurvivin treatment ($n = 4$ per group). (**a**) Inflammatory cytokine level (IL-6 level) analyzed at 6 h after LDH-FA/siSurvivin treatment, (**b**) ALT and AST levels, and (**c**) H&E staining of liver tissues performed on day 3 after treatment (original magnification: × 100) (after Park et al., 2016, reproduced with the permission of Wiley)

The exfoliation-reassembling process is also suggested as a useful way of encapsulating or intercalating bulky and large-sized biomolecules into lamellar clays, whether they are cationic or anionic. If the layer charge were not that big, the multilayers consisting of cationic or anionic layers could be exfoliated into a single layer by intercalating polar solvent molecules (Mnt: e.g. ammonium salts with long alkyl chains, polymer natrix; LDH: e.g. formamide) (James et al. 2015; Ma et al. 2006). Once exfoliated, they are then allowed to reassemble in the presence of guest molecules in a solution. In this way guest molecules can be intercalated into the clay lattice to build the clay hybrid with 1:1 heterostructure.

The final route to clay hybrids is the calcination-reconstruction process. Thanks to the structural memory effect of LDHs, the pristine Mg-Al LDH is, at first, calcined at ~400–500°C in such a way that layered metal hydroxide is thermally decomposed into amorphous metal oxides along with a weakly developed periclase MgO phase (JCPDS 43–1022), followed by dehydration and subsequent dehydroxylation reactions. An amorphous oxide phase prepared in this manner can be recrystallized into LDH upon rehydration. If the rehydration reaction occurs in the presence of guest molecules in a solution, the clay hybrid can simply be regenerated.

CLAY MINERALS IN MEDICINAL APPLICATIONS

Oral medicine

Various drugs such as antimalaria (Kim et al., 2015), anti-psychotic (Oh et al., 2013), antibiotic (Jung et al. 2008; Yang et al. 2013; Ghadiri et al. 2014), and anti-cancer (Kevadiya et al., 2012; Iliescu et al., 2014; Massaro et al., 2015) have been explored extensively for oral administration, but some were found to have drawbacks such as low bioavailability, poor water solubility, unpleasant taste, etc. In order to overcome such issues, advanced drug delivery systems with suitable delivery carriers are required urgently. Amongst various drug delivery carriers, clay minerals were considered as promising because the drug molecules can be incorporated into the interlayer of montmorillonite by an intercalative ion-exchange reaction, or into the nanotube of halloysite by capillary condensation, and also released from the drug-clay hybrid into a body fluid. Clay minerals, moreover, were found to be biocompatible with low toxicity, large drug-loading capacity, and sustained-release property.

Several approaches have been made to develop drug-clay hybrids for oral medications (Table 3). Oh et al. (2013), for example, reported an aripiprazole (APZ)-montmorillonite (Mnt) hybrid, which was further encapsulated with

https://doi.org/10.1007/s42860-019-0009-9 Published online by Cambridge University Press

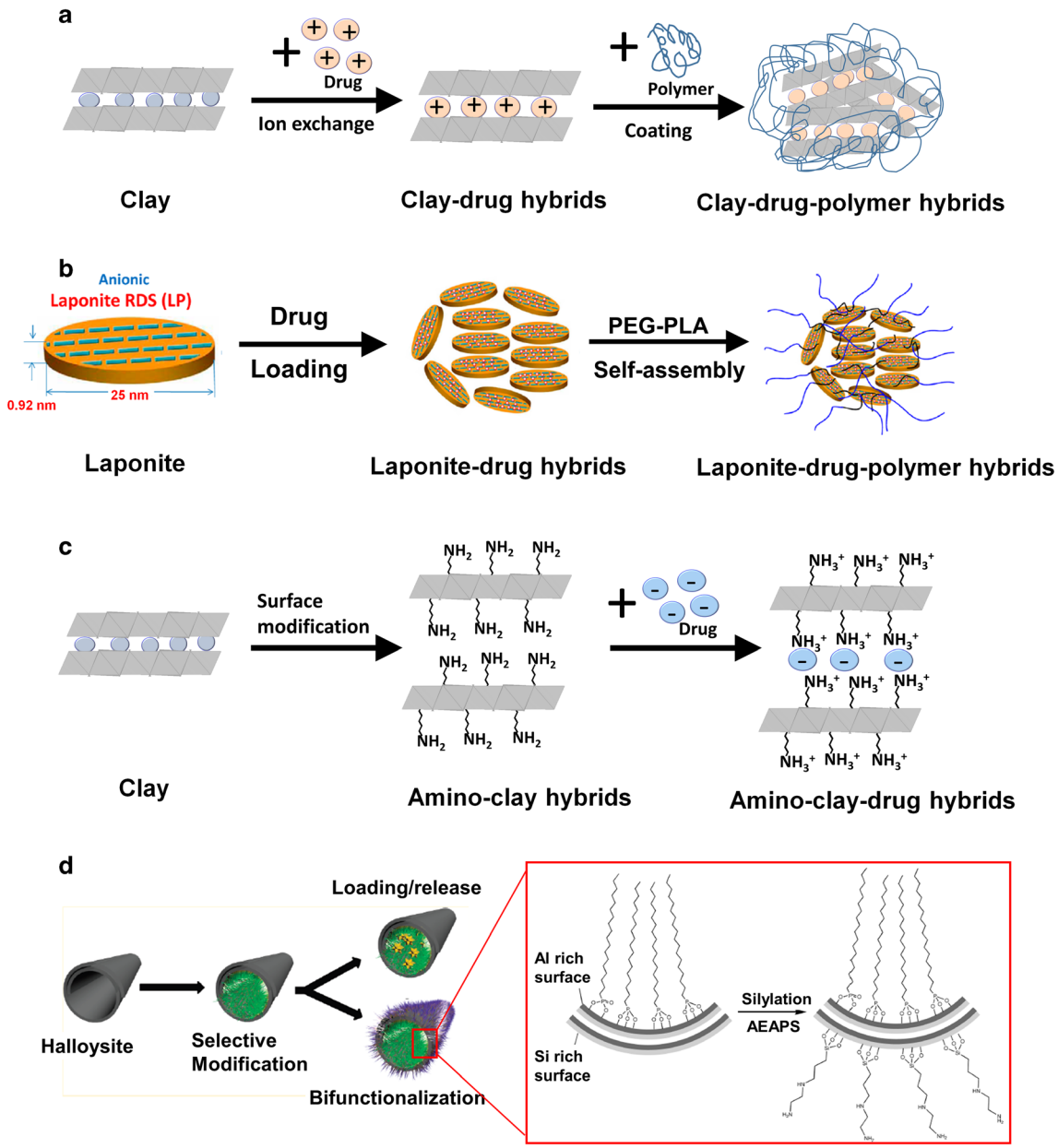

Fig. 6 Chemical modifications of clay hybrid materials. Schematic procedures for (**a**) polymer coating on clay-drug nanohybrid, (**b**) self-assembling of Laponite®-drug hybrid with polymer (after Wang et al., 2018), (**c**) immobilizing drug molecules in aminoclay nanohybrid, and (**d**) bifunctionalizing internal and external surfaces of halloysite nanotubes (after Yah et al., 2012, reproduced with the permission of the American Chemical Society)

polyvinylacetal diethyl-amino acetate (AEA) in order to overcome the poor aqueous solubility and unpleasant taste of aripiprazole (APZ: 7-{4-[4-(2,3-dichlorophenyl)piperazin-1-yl]butoxy}-3,4-dihydro quinolin-2(*1H*)-one). APZ has been used widely for treating the negative and positive symptoms of schizophrenia with reduced extrapyramidal side effects compared to the control drug, the commercially used tablet for oral delivery (Abilify®, Otsuka Pharmaceutical) (Oh et al., 2013; Harrison & Perry, 2004; Green, 2004) According to in vitro dissolution tests at neutral pH (Fig. 8A(a)), APZ drug release from AEA-coated APZ-Mnt was greatly reduced (<1%) for up to 3 min, thus masking the taste of the APZ. In a simulated gastric solution at pH 1.2, however, the total percentage of APZ released over a 2 h period was up to 95% in the case of AEA-coated APZ-Mnt (Fig. 8A(b)). The release profile of APZ in vitro was the same as from the Abilify®, indicating that the present formulation of AEA-coated APZ-Mnt could be developed further as a new generic drug or an incrementally modified new drug (IMD). Kim et al. (2015) studied an antimalarial drug (artesunic acid; ASH), which orally, has poor bioavailability as the aqueous solubility of ASH is extremely low. To overcome this

https://doi.org/10.1007/s42860-019-0009-9 Published online by Cambridge University Press

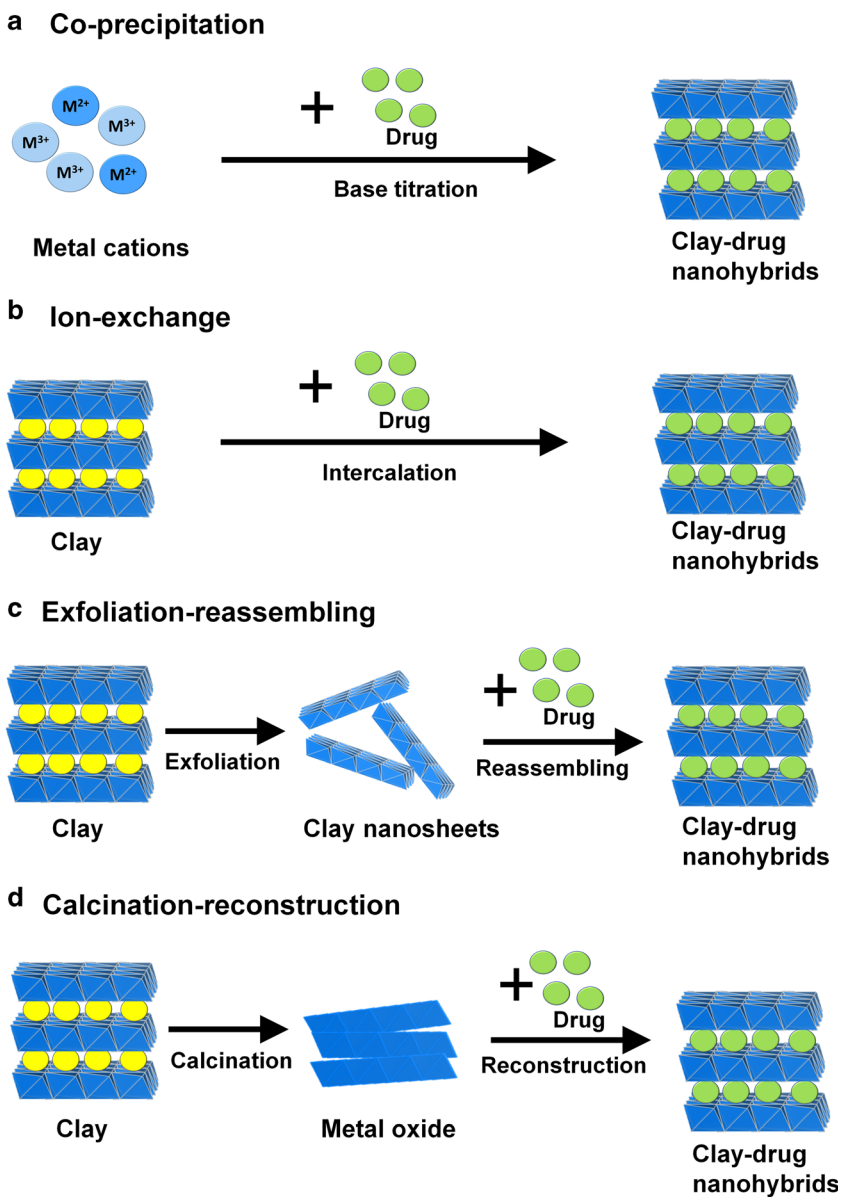

Fig. 7 Reaction routes for clay hybrid materials; (**a**) co-precipitation, (**b**) ion-exchange, (**c**) exfoliation-reassembling, and (**d**) calcination-reconstruction

problem, artesunate (AS) was immobilized in the ZBS interlayer space by the co-precipitation method, and then further coated with Eudragit® L100. According to the in vivo pharmacokinetic results (Fig. 8B(a)), the AS level was considerably higher in the rat plasma administered with Eudragit® L100-coated AS-ZBS than with pure ASH. When the Eudragit® L100-coated AS-ZBS nanohybrid was administered orally, the AUC parameter of Eudragit® L100-coated AS-ZBS was determined to be 5.5 times larger than that of intact ASH. Eudragit® L100-coated AS-ZBS can, therefore, be recommended as a hybrid drug-delivery system for enhancing drug solubility and bioavailability (Kim et al., 2015). Many previous reports including the two mentioned above have confirmed that cationic and anionic clays can play a role as drug delivery carriers and their nanohybrids can provide a novel drug delivery platform of oral medication for taste masking, solubility enhancement, bioavailability enhancement, and sustained and controlled release.

Injectable medicine

As already suggested by Choy's group (Oh et al. 2006, 2009), the ~100 nm-sized LDH nanoparticles are, in general, biocompatible and targetable to tumor tissues and cells, not only due to their particle-size-dependent tissue-targeting function, ascribed to their enhanced permeability and retention (EPR) effects, but also due to their intrinsic cell targeting function known as the

https://doi.org/10.1007/s42860-019-0009-9 Published online by Cambridge University Press

https://doi.org/10.1007/s42860-019-0009-9 Published online by Cambridge University Press

Table 3 Summary of oral medicine using clay minerals

Species	Drug	In vitro and in vivo study	Application	Reference
ZBS	Artesunate (AS)	In vivo pharmacokinetic study	- Eudragit® L100-coated AS-ZBS - Bioavailability enhancement	Kim et al. (2016)
Mg_2Al-LDH	Ursodeoxycholic acid (UDCA)	In vitro release test	- Eudragit® S100-coated UDCA-LDH - Solubility enhancement	Choi et al. (2013)
ZBS Zn_2Al-LDH	Indole-3-acetic acid (IAA)	In vitro release test	- Sustained release	Yang et al. (2014)
Mnt	Telmisartan (TEL)	In vivo pharmacokinetic study	- 3-Aminopropyl functionalized magnesium phyllosilicate (aminoclay) - Bioavailability enhancement	Yang et al. (2013)
Mnt	Irinotecan	In vitro release test	- Montmorillonite-alginate nanocomposite - Controlled release	Iliescu et al. (2014)
Mnt	Itraconazole (ITA)	In vivo pharmacokinetic study	- Solubility enhancement - Bioequivalence drug	Yang et al. (2007)
Mnt	Aripiprazole (APZ)	In vivo pharmacokinetic study	- Taste masking - Solubility enhancement - Sustained release	Oh et al. (2013)
Mnt	Sildenafil (SDN)	In vivo pharmacokinetic study	- Taste masking	Lee et al. (2012)
Mnt	Tamoxifen (Tmx)	In vivo pharmacokinetic study	- Montmorillonite/poly-(ε-caprolactone) composites - Controlled release	Kevadiya et al. (2012)
Laponite®	Tetracycline	In vitro release test	- Sustained release	Ghadiri et al. (2013)
Laponite®	Itraconazole (ITA)	In vitro release test	- Solubility enhancement - Controlled release	Jung et al. (2008)
Halloysite	Cardanol	Cytotoxicity test	- Cytotoxic effects	Massaro et al. (2015)
Halloysite	Amoxicillin	In vitro release test	- Sustained release	Wei et al. (2014)

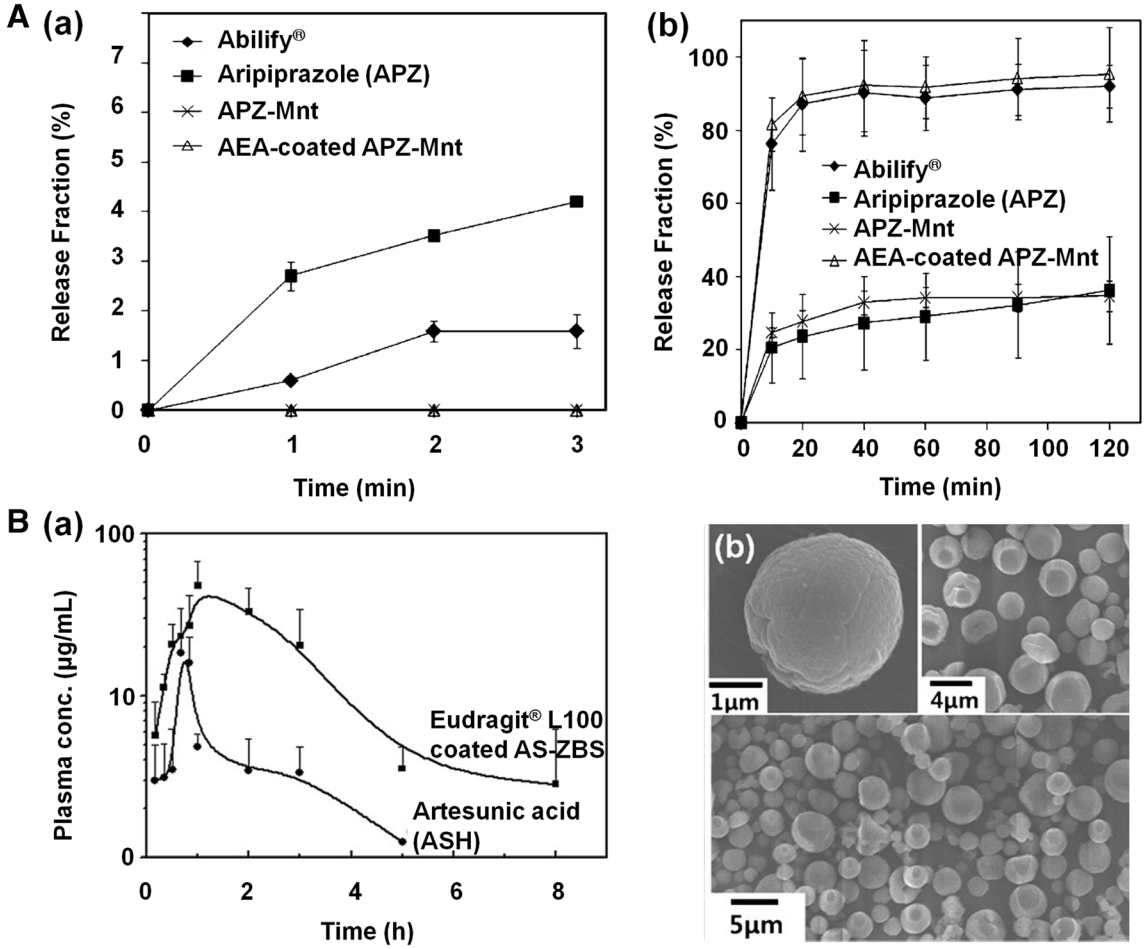

Fig. 8 (**A**) Release profiles of APZ (a) in deionized water with 1% Tween 80, and (b) in simulated gastric fluid (pH 1.2) with 1% Tween 80 (modified from Oh et al., 2013). (**B**) Pharmacokinetic curves of AS after oral administration (a), and scanning electron microscopy (SEM) images of Eudragit® L100-coated AS-ZBS (b) (after Kim et al., 2016, reproduced with the permission of Wiley)

intercellular pathway based on the clathrin-mediated endocytosis mechanism.

Many attempts have been made to develop LDH nanoparticles using injectable medicine for chemo-, gene-, and

Table 4 Summary of injectable medicine using clay minerals

Species	Drug	In vivo animal model	Application	Reference
Mg_2Al-LDH	Methotrexate (MTX)	Xenograft osteosarcoma (HOS) mice model	Chemotherapy	Choi et al. (2010)
		Orthotopic breast cancer (MCF-7/mot) mice model	Chemotherapy	Choi et al. (2014)
		Orthotopic cervical cancer (C33A) mice model	Chemotherapy	Choi et al. (2012)
		Xenograft osteosarcoma (HOS) mice model	Chemotherapy	Ray et al. (2017)
Zn_2Al-LDH	Mercaptoundecahydrocloso-dodecaborate (BSH)	Xenograft glioblastoma (U87) mice model	Boron Neutron Capture Therapy (BNCT)	Choi et al. (2017)
Mg_2Al-LDH	Survivin siRNA	Xenograft carcinoma (KB) mice model	Gene therapy	Park et al. (2016)
Halloysite nanotubes	Doxorubicin (DOX)	Xenograft breast cancer (4 T1) mice model	Chemotherapy	Wen et al. (2015)

https://doi.org/10.1007/s42860-019-0009-9 Published online by Cambridge University Press

radiation-therapy (Table 4). Choy, Oh, and co-workers, for example, were successful in encapsulating methotrexate (MTX), an anticancer drug, in an LDH delivery vehicle to prepare a potential DDS as an MTX-LDH nanohybrid with a particle size of ~100 nm (Choi et al. 2012, 2013, 2014, 2016; Oh et al., 2006). According to the Trypan Blue assay, the cell viability with MTX-LDH was more significantly reduced than that with intact MTX. The IC_{50} value for intact MTX in osteosarcoma MNNG/HOS cells was determined to be ~2.5 times greater than that for MTX-LDH, suggesting that the latter could permeate through the cell membrane more efficiently than the former, resulting in improved drug delivery, and eventually higher drug efficacy. The cell viability, furtheremore, was not significantly influenced by the concentrations of LDH nanoparticles up to concentrations of 500 μg/mL (Oh et al., 2006), indicating its low cytotoxicity. Choi et al. (2014) also prepared an injectable MTX-LDH nanohybrid system by the co-precipitation route, and examined drug efficacy for the first time in an orthotopic breast cancer model. According to the biodistribution studies, the mice injected with MTX-LDH showed that six times more MTX was delivered to the tumor than those treated with intact MTX, indicating the tumor targeting function of the drug delivery vehicle, LDH. Furthermore, an MTX-LDH nanohybrid showed better drug efficacy than intact MTX in a tumor growth inhibition test with the same orthotopic mice model (Choi et al., 2014). More recently, Choi et al. (2017) studied an injectable LDH nanovehicle hybridized with mercaptoundecahydroclosododecaborate (BSH) for boron neutron capture therapy (BNCT). According to the biodistribution studies in the xenograft glioblastoma (U87) mice model (Fig. 9a), the tumour MTX-to-blood MTX ratio of BSH in the BSH-LDH-treated-group was found to be 4.4 times greater than that in the intact BSH-treated group 2 h after drug treatment (Choi et al., 2017). Such a targeting phenomenon in vivo can be explained not only by the enhanced permeability and retention (EPR) effect of the nanosized BSH-LDH particles (~100 nm), which deliver BSH molecules preferentially to tumor tissue and eventually to tumor cells, but also by their excellent cellular uptake effect due to clathrin-mediated endocytosis (Oh et al., 2006).

In the case of cationic clays, however, only a few studies have been done on injectable drug-clay systems, no doubt because of the difficulties in controlling particle sizes at <100 nm, and the insolubility in body fluid resulting in problems of organ accumulation after injection. However, Wu et al. (2018) reported recently the use of folate-conjugated halloysite nanotubes (HNTs) for doxorubicin (DOX) delivery. The particle size of HNTs was controlled at 200 nm by ultrasonic scission, and thus prepared, nanoparticles were functionalized with amide groups to

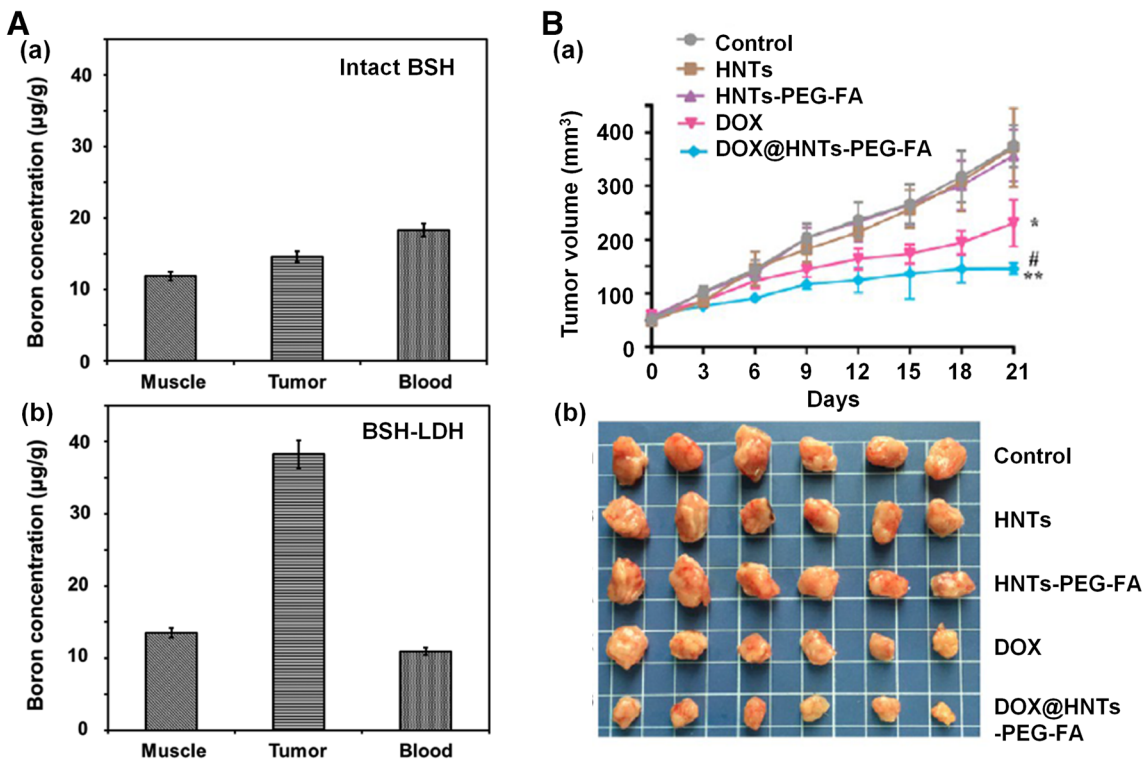

Fig. 9 **A** Biodistribution studies of boron in each tissue of U87 xenograft tumor-bearing mice treated with (a) BSH and (b) BSH-LDH for 2 h after administration (after Choi et al., 2017). **B** Antitumor effects of DOX@HNTs-PEG-FA in four T1-bearing mice; (a) tumor growth curves of mice treated with saline, HNTs, HNTs-PEG-FA, DOX, and DOX@HNTs-PEG-FA (5 mg DOX equiv./kg) via intravenous injection, and (b) photographs of excised 4 T1 solid tumor from different groups on the 22nd day. The values are represented as mean ± SD ($n = 6$). $^{*}P < 0.05$, $^{**}P < 0.01$, vs. control; $^{\#}P < 0.05$ vs. DOX (after Wen et al. 2015, reproduced with the permission of the Royal Society of Chemistry)

https://doi.org/10.1007/s42860-019-0009-9 Published online by Cambridge University Press

induce chemical bonding with N-hydroxylsuccinimide-polyethylene glycol carboxylic acid (NHS-PEG-COOH) and folate (FA). DOX@HNTs-PEG-FA was then synthesized by adding DOX on HNTs-PEG-FA via simple physical adsorption. According to the in vivo studies, an antitumor effect of DOX@HNTs-PEG-FA was clearly confirmed in a breast cancer (4 T1 cells) mice model through intravenous injection. As expected, the tumor volume and tumor weight in 4 T1-bearing mice for both cases, DOX ($P < 0.05$) and DOX@HNTs-PEG-FA ($P < 0.01$) treatments, were strongly reduced with respect to the control group, while no significant change could be observed for the HNTs and HNTs-PEG-FA treatment groups (Fig. 9B) (Wu et al., 2018). Even though HNT is non-degradable, it was used as a drug delivery carrier due to its low toxicity in vivo (Wu et al., 2018). However, a long-term biodistribution study is required to follow its trafficking pathways and to understand its fate after injection.

Diagnostics

The diagnosis of cancer can be made using a variety of molecular imaging techniques such as magnetic resonance imaging (MRI), computerized tomography (CT), nuclear imaging including positron emission tomography (PET), single photon emission computed tomography (SPECT), and optical imaging, etc. For precise cancer diagnosis, various inorganic and/or organic materials, including liposome, dendrimer, and clay minerals immobilized with imaging agents have been developed (Xing et al. 2016; Cheng et al. 2011; Choi et al., 2018). Various clay minerals such as montmorillonite (Mnt), Laponite®, halloysite, and layered double hydroxide have already been explored as carriers of molecular imaging agents for diagnostics (Table 5).

Nuclear molecular imaging

Radiology was started after the discovery of X-rays by Roentgen in 1895, and nuclear medicine began after the discovery of radium and its radioactivity by Becquerel and the Curies in 1896. In nuclear medicine, the gamma camera was developed by Anger in 1958 for tomographic imaging, and today it is used in the form of SPECT and PET (McRobbie et al. 2017). The detection sensitivity of SPECT and PET is very high, even at very low concentrations with a picomolar or a nanomolar range (Khalil et al. 2011). The imaging agents for SPECT are, in general, doped with radioisotopes, such as ^{99m}Tc, ^{111}In, ^{123}I, ^{57}Co, and ^{67}Ga, which can emit gamma rays. On the other hand, radioisotopes emitting positrons are employed for PET, and the positron emitters known so far are: ^{15}O, ^{13}N, ^{11}C, ^{18}F, ^{64}Cu, and ^{68}Ga (Gambhir, 2002). PET images can be made from high-energy gamma-rays emitted by annihilation between electrons and positrons upon decay of the radioactive isotope (Fig. 10). For example, decay of ^{11}C can be represented by the following equation: $^{11}_{6}C \rightarrow {}^{11}_{5}B + e^{+}$ (positron) + ν_e (neutrino). The positron thus emitted happens to meet an electron from the surrounding environment after decaying, and then these two particles, e^{+} and e^{-}, combine and 'annihilate' each other generating two 0.511 MeV gamma-rays in opposite directions (Fig. 10a). A PET scan can detect these two gamma-rays, and then images can be represented by showing the positions and concentration of the imaging agent (Fig. 10B(a)). Finally, cross-sectional PET images for coronal, transverse, and sagittal planes can be obtained (Fig. 10B(b)). Radioisotopes themselves have an imaging function, however, not a targeting function to malignant tissues and cells. Exploring new carriers with a targeting function to immobilize gamma ray or positron emitters is, therefore, necessary.

As described above, clay minerals doped with a radioisotope were explored for in vitro and in vivo diagnostics for tumors (Table 5). Sarcinelli et al. (2016), for example, investigated detection of breast cancer using polylactic acid (PLA)/polyvinyl alcohol (PVA)/montmorillonite (Mnt)/trastuzumab nanoparticles labeled with ^{99m}Tc. The targeting property of LDH with ^{57}Co incorporated through isomorphous substitution was shown in an animal experiment with the CT-26 (colon

Table 5 Clay minerals as carriers of molecular imaging agents for nanomedicine

Imaging type	Clay type	Imaging agent	Reference
Nuclear Image (SPECT/PET)	Montmorillonite	Tc-99 m	Sarcinelli et al. (2016)
	Layered Double Hydroxide	Cu-64	Shi et al. (2015)
	Layered Double Hydroxide	Co-57	Kim et al. (2016)
MRI	Laponite®	Fe_2O_3	Ding et al. (2016)
	Halloysite	Fe_2O_3	Zhou et al. (2016)
	Layered Double Hydroxide	Gd	Wang et al. (2014)
CT	Laponite®	Au	Zhuang et al. (2017)
	Layered Double Hydroxide	Au	Wang et al. (2014)
Fluorescence	Laponite®	DOX	Zhuang et al. (2017)
	Halloysite	Eu	Zhou et al. (2016)
	Layered Double Hydroxide	FITC	Park et al. (2016)

https://doi.org/10.1007/s42860-019-0009-9 Published online by Cambridge University Press

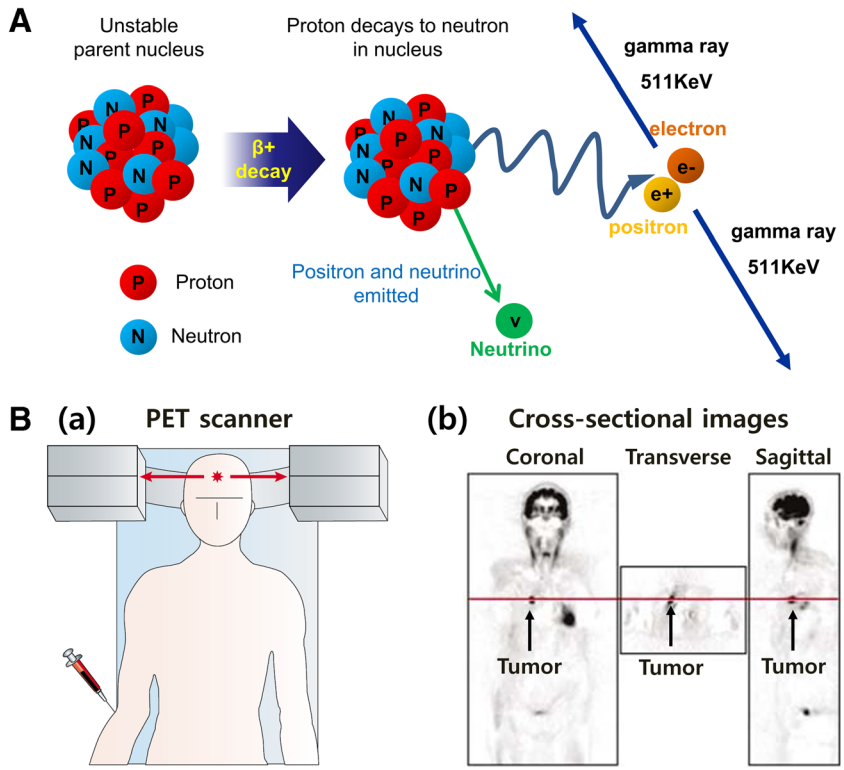

Fig. 10 **A** Positron emission from radioisotope. **B** (a) Positron emission tomography (PET) scanner and (b) cross-sectional PET image after injection with 2-[^{18}F]fluoro-2-deoxy-D-glucose (FDG) (after Gambhir (2002, reproduced with the permission of Nature Reviews))

carcinoma cell) xenografted mice model (Kim et al. 2016). According to the in vivo biodistribution study, the radioisotope could clearly be delivered selectively to the tumor, thanks to the LDH carrier. Such experimental results indicate that the radioisotope-labeled clay product can be suitable as a cancer imaging agent.

Magnetic Resonance Imaging (MRI)

Magnetic resonance imaging (MRI) is a medical imaging technique employed to obtain information about the anatomy and the physiological processes of the patient body. Unlike CT scanning, MRI is not related to any strong ionizing radiation, and its scanners use only strong magnetic fields, electric field gradients, and radio waves to produce images of the organs in the body (Bushong et al., 2014). MRI has significantly higher resolution than SPECT and PET, while its sensitivity is very low in comparison (Table 6) (Khalil et al., 2011).

In the MR image, the differences in proton density result in MRI contrast in soft tissue; the two modes are: T_1 (spin-lattice relaxation time) and T_2 (spin-spin relaxation time) of protons. The former is also called longitudinal relaxation, which is related to how rapidly the magnetization is recovered parallel to the magnetic field after a RF pulse. Protons that relax rapidly (short T_1) recover magnetization completely along the longitudinal axis and generate large signal intensities. For protons which relax more slowly (long T_1), magnetization cannot be recovered fully before subsequent RF pulses and, therefore, inherently produce less signal. T_1-weighted images are well demonstrated in anatomy, and are the preferred option when a clear image of a structure is needed (Stephen, Kievit, & Zhang,

Table 6 Important parameters for different imaging technologies (after Dufort et al. 2010, reproduced with the permission of Elsevier; Data from Korea Institute of Radiological & Medical Sciences)

Technique	Resolution	Depth	Time	Sensitivity
PET	1–2 mm	No limit	Minutes	10^{-11} – 10^{-12} M
SPECT	1–2 mm	No limit	Minutes	10^{-10} – 10^{-11} M
MRI	10–100 μm	No limit	Minutes–hours	10^{-3} – 10^{-5} M
CT	< 50 μm	No limit	Minutes	Not well characterized
Fluorescence	1–2 mm	< 1 cm	Seconds	Not well characterized

https://doi.org/10.1007/s42860-019-0009-9 Published online by Cambridge University Press

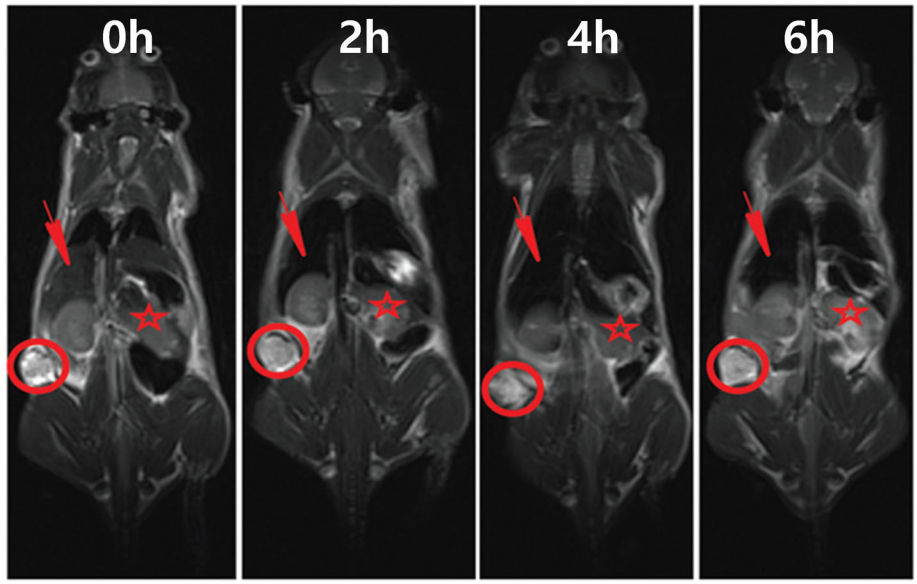

Fig. 11 In vivo T_2-weighted MR images of tumor (red circle), liver (red arrow), and kidney (red star) after intravenous injection of Laponite®-Fe_3O_4 nanoparticles for 0 h, 2 h, 4 h, and 6 h (after Ding et al. 2016, reproduced with the permission of the Royal Society of Chemistry)

2011). T_2 relates to how fast the in-plane magnetization vertical to the static magnetic field loses coherence, as represented by transverse relaxation. Upon a RF pulse, proton nuclei spin in-phase. After the pulse, however, the magnetic fields of all the

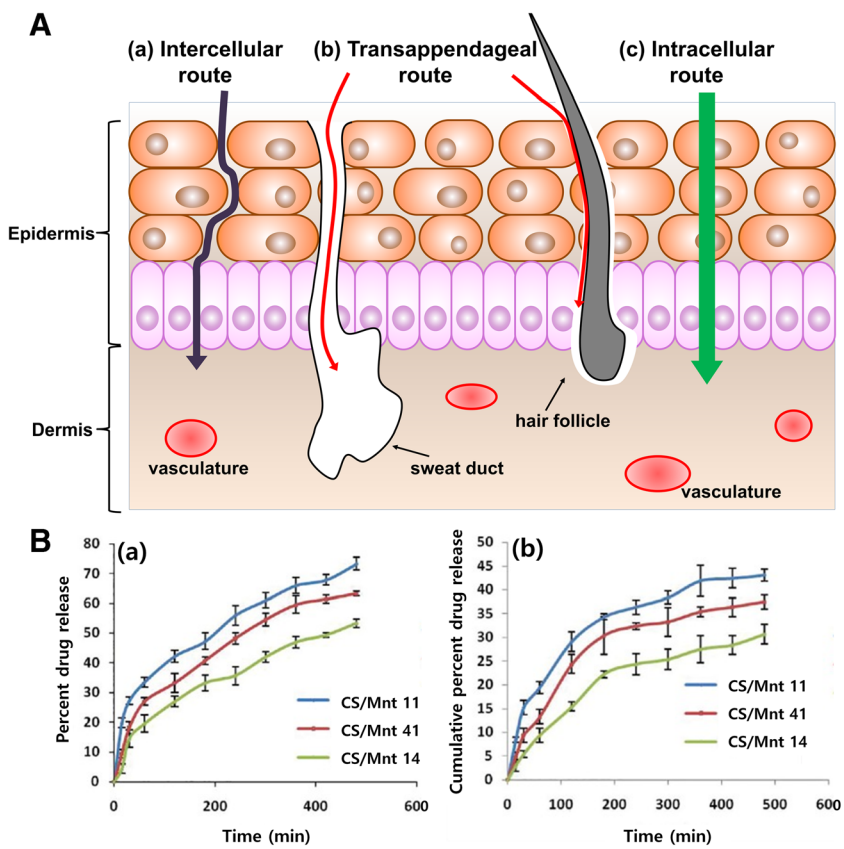

Fig. 12 (**A**) Different transdermal pathways of clay nanoparticles. (**B**) (a) In vitro drug release, and (b) permeation behaviors of the chitosan/montmorillonite K transdermal films (after Thakur et al., 2016, reproduced with the permission of Wolters Kluwer Medknow Publications)

https://doi.org/10.1007/s42860-019-0009-9 Published online by Cambridge University Press

nuclei interact with each other, and, as a consequence, energy is exchanged between them. The nuclei lose their phase coherence and eventually tend to spin in a random fashion (Estelrich, Sánchez-Martín, & Busquets, 2015).

High-spin paramagnetic metals such as gadolinium (Gd^{3+}), manganese (Mn^{2+}), or iron (Fe^{3+}) are used commonly as T_1 contrast agents, while ferro- and ferrimagnetic or superparamagnetic materials such as iron oxide (Fe_3O_4) have been used as T_2 contrast agents. These T_1 and T_2 contrast agents themselves do not show any targeting effect, and they are also excreted quickly by short blood circulation time in the body due to small particle sizes (<50 nm). As a result, clay minerals (Laponite®, halloysite, and LDH) immobilized with MR contrast agents have been studied for MR imaging in order to improve the passive targeting effect and blood circulation time (Table 5). After hybridizing commercially available Laponite® clay with superparamagnetic Fe_3O_4 nanoparticles having large T_2 relaxivity, the Laponite®-Fe_3O_4 hybrid was injected into the HeLa (human cervical carcinoma cell) xenograft mice model. Surprisingly, bright and dark MR images were observed, respectively, in tumor and liver tissues after 2 h, 4 h, and 6 h (Fig. 11) (Ding et al., 2016). LDH clay was also doped with Gd^{3+} ions (LDH-Gd), well known as a MR contrast agent, and demonstrated on 4 T1 murine breast tumor-bearing mice for T_1-weighted MR images related to the spin-lattice relaxation mode. MR signal intensity of LDH-Gd was increased gradually from 4688.7 to 4904.5 and 5166.7, respectively, 1 h and 4 h after injection, indicating that LDH-Gd could be an effective MR imaging system for tumors (Wang et al., 2013). In conclusion, clay minerals, whether they are cationic or anionic, are potential carriers for MR contrasting agents due to their biocompatibility and passive targeting effect.

Transdermal medicine

Transdermal delivery refers to delivery of drug molecules across the skin into the blood circulation at a fixed rate (Marwah, Garg, Goyal, & Rath, 2016; Lee et al., 2017). Three routes are possible for drug delivery across intact skin, namely the intercellular, intracellular, and trans-appendiceal pathways (Fig. 12a). The intercellular and intracellular pathways involve passage through the stratum corneum, an architecturally diverse, multi-layered, and multi-cellular barrier. The intercellular route is the common pathway, allowing diffusion of lipophilic or non-polar solutes across the continuous lipid matrix. The intracellular route through corneocytes, terminally differentiated keratinocytes, however, allows the transportation of hydrophilic or polar solutes. The transappendageal route is related to passage through sweat glands and across hair follicles, which provides a continuous channel for drug permeation but is blocked easily due to the presence of hair follicles and sweat ducts (Alkilani et al. 2015; Marwah et al., 2016). In practice, transdermal patches have been developed as adhesive ones that can be attached to the skin. The polymer matrix is one of the main components of the patch due to its flexibility and drug reservoir property (Prausnitz et al., 2008). To give an effective drug delivery property for transdermal medicine, the design of the drug delivery systems not only to have large drug-loading capacity but also to have sustained drug release behavior is very important. For this reason, clay minerals have been in the spotlight due to their large drug-loading capacity and controlled release behavior in the body fluid systems.

Chitosan/montmorillonite K 10 (CS/Mnt) clay minerals were prepared as a transdermal film type for curcumin delivery (Thakur et al. 2016). According to the release study of curcumin from the CS/Mnt films (Fig. 12B(a), the sustained release could be observed in three cases: 53.34 ± 1.26%, 63.23 ± 1.56%, and 73.27 ± 1.71% for CS/Mnt 14, 41, and 11, respectively (where 14, 41, and 11 indicate the ratios between CS and Mnt (1:4, 4:1, and 1:1)). For in vitro drug permeation studies of CS/Mnt films, CS/Mnt 11, CS/Mnt 41, and CS/Mnt 14 were used on rat skin with a size of 1 cm^2 for 24 h. The drug releases of CS/Mnt 11, CS/Mnt 41, and CS/Mnt 14 films were 30.63 ± 2.04%, 37.45 ± 1.49%, and 43.03 ± 1.09%, respectively, after 8 h of permeation (Fig. 12B(b)). As a result, a permeation efficacy of 59% was found for the CS/Mnt 14 film, indicating that drug molecules indeed penetrated the skin by their controlled-release properties. In conclusion, a patch (or film) containing a drug-clay hybrid could be suggested as a promising transdermal material for biomedicine.

SUMMARY AND PERSPECTIVES

Clay minerals, including a variety of cationic and anionic clays, have been used as delivery carriers of therapeutic and diagnostic agents for nanomedicine including oral, injectable, and transdermal medications, etc. Depending on the nanomedical applications, clay minerals could be designed and functionalized by various synthetic routes and their special parameters eventually optimized, such as size, dispersibility, drug-release property, and chemical- and biostability, etc. Based on much experimental evidence from in vitro and in vivo studies as described in this tutorial review, such a proof of concept of clay delivery carriers has great implications for actual future application in nanomedicine. Many challenges remain, however, because the long-term in vivo evaluations of therapeutic efficacy and diagnostic properties, including bio-distributions and excretion mechanisms, of clay nanoparticles should be done under clinical-trial conditions, and their long-term toxicology studies are also needed.

ACKNOWLEDGMENTS

This work was supported by the National Research Foundation of Korea (NRF) Grants funded by the Korean Government (MSIP) (No. 2017R1A6A3A11034149, No. 2016R1D1A1A02937308, and No. 2017K2A9A2A10013104).

REFERENCES

Alkilani, A.Z., McCrudden, M.T., & Donnelly, R.F. (2015). Transdermal drug delivery: innovative pharmaceutical developments based on disruption of the barrier properties of the stratum corneum. *Pharmaceutics, 7*, 438–470.

Baek, M., Lee, J.A., & Choi, S.J. (2012). Toxicological effects of a cationic clay, montmorillonite in vitro and in vivo. *Molecular & Cellular Toxicology, 8*, 95–101.

https://doi.org/10.1007/s42860-019-0009-9 Published online by Cambridge University Press

Bergaya, F. and Lagaly, G. (2006). General introduction: clays, clay minerals and clay science. In: Handbook of Clay Science (F. Bergaya, B.K.G. Theng, & G. Lagaly, eds.), pp. 1–18. Developments in Clay Science, 1, Elsevier, Amsterdam.

Biswick, T., Park, D.H., Shul, Y.G., & Choy, J.H. (2009). P-coumaric acid–zinc basic salt nanohybrid for controlled release and sustained antioxidant activity. *Journal of Physics and Chemistry of Solids, 71*, 647–649.

Bull, R.M.R., Marklan, C., Williams, G.R., & O'Hare, D. (2011). Hydroxy double salts as versatile storage and delivery matrices. *Journal of Materials Chemistry, 21*, 1822–1828.

Bushong, S.C. and Clarke, G. (2014). *Magnetic resonance imaging: physical and biological principles*. Elsevier Health Sciences, Amsterdam, pp. 2–16.

Cheng, Y., Zhao, L., Li, Y., and Xu, T. (2011). Design of biocompatible dendrimers for cancer diagnosis and therapy: current status and future perspectives. *Chemical Society Reviews, 40*, 2673–2703.

Choi, G., Eom, S., Vinu, A., & Choy, J.H. (2018). 2D nanostructured metal hydroxides with gene delivery and theranostic functions; a comprehensive review. *The Chemical Record, 18*, 1–22.

Choi, G., Jeon, I.R., Piao, H., & Choy, J.H. (2017). Highly condensed boron cage cluster anions in 2D carrier and its enhanced antitumor efficiency for boron neutron capture therapy. *Advanced Functional Materials,* 1704470.

Choi, G., Kim, S.Y., Oh, J.M., & Choy, J.H. (2012). Drug-ceramic 2-dimensional nanoassemblies for drug delivery system in physiological condition. *Journal of the American Ceramic Society, 95*, 2758–2765.

Choi, G., Kwon, O., Oh, Y., Yun, C.O., & Choy, J.H. (2014). Inorganic nanovehicle targets tumor in an orthotopic breast cancer model. *Scientific Reports, 4*, 4430.

Choi, G., Lee, J.H., Oh, Y.J., Choy, Y.B., Park, M.C., Chang, H.C., & Choy, J.H. (2010). Inorganic-polymer nanohybrid carrier for delivery of a poorly-soluble drug, ursodeoxycholic acid. *International Journal of Pharmaceutics, 402*, 117–122.

Choi, S.J., Oh, J.M., & Choy, J.H. (2008). Safety aspect of inorganic layered Nanoparticles: size-dependency in vitro and in vivo. *Journal of Nanoscience and Nanotechnology, 8*, 529–5301.

Choi, S.J., Oh, J.M., Chung, H.E., Hong, S.H., Kim, I.H., & Choy, J.H. (2013). In vivo anticancer activity of methotrexate-loaded layered double hydroxide nanoparticles. *Current Pharmaceutical Design, 19*, 7196–7202.

Choi, S.J., Oh, J.M., Park, T., & Choy, J.H. (2007). Cellular toxicity of inorganic hydroxide nanoparticles. *Journal of Nanoscience and Nanotechnology, 7*, 4017–4020.

Choi, G., Piao, H., Alothman, Z.A., Vinu, A., Yun, C.O., & Choy, J.H. (2016). Anionic clay as the drug delivery vehicle: tumor targeting function of layered double hydroxide-methotrexate nanohybrid in C33A orthotopic cervical cancer model. *International Journal of Nanomedicine, 11*, 337–3487.

Choy, J.H. (2004). Intercalative route to heterostructured nanohybrid. *Journal of Physics and Chemistry Solids,* **65**, 373–383.

Choy, J.H., Kwak, S.Y., Jeong, Y.J., & Park, J.S. (2000). Inorganic layered double hydroxide as a non-viral vector. *Angewante Chemie International Edition, 39*, 4042–4045.

Choy, J.H., Kwak, S.Y., Park, J.S., Jeong, Y.J., & Portier, J. (1999). Intercalative nanohybrids of nucleoside monophosphates and DNA in layered metal hydroxide. *Journal of the American Chemical Society,* **121**, 1399–1400.

Demir, F., Demir, B., Yalcinkaya, E.E, Cevik, S., Demirkol, D.O., Anik, U., & Timur, S. (2014). Amino acid intercalated montmorillonite: electrochemical biosensing applications. *RSC Advances, 4*, 50107–50113.

Ding, L., Hu, Y., Luo, Y., Zhu, J., Wu, Y., Cao, X., Peng, C., Shi, X., & Guo, R. (2016). Laponite®-stabilized iron oxide nanoparticles for in vivo MR imaging of tumors. *Biomaterials Science, 4*, 474–482.

Dufort, S., Sancey, L., Wenk, C., Josserand, V., & Coll, J.L. (2010). Optical small animal imaging in the drug discovery process. *Biochimica et Biophysica Acta (BBA)-Biomembranes, 1798*, 2266–2273.

Estelrich, J., Sánchez-Martín, M.J., & Busquets, M.A. (2015). Nanoparticles in magnetic resonance imaging: from simple to dual contrast agents. *International Journal of Nanomedicine, 10*, 1727–1742.

Gaharwar, A.K., Mihaila, S.M., Swami, A.S., Patel, A., Sant, S., Reis, R.L., Marques, A.P., Gomes, M.E., & Khademhosseini, A. (2013). Bioactive silicate nanoplatelets for osteogenic differentiation of human mesenchymal stem cells. *Advanced Materials, 25*, 3329–3336.

Gambhir, S.S. (2002). Molecular imaging of cancer with positron emission tomography. *Nature Reviews Cancer, 2*, 683–693.

Ghadiri, M., Chrzanowski, W., & Rohanizadeh, R. (2014). Antibiotic eluting clay mineral (Laponite®). for wound healing application: an in vitro study. *Journal of Materials and Science, 25*, 2513–2526.

Ghadiri, M., Hau, H., Chrzanowski, W., Agus, H., & Rohanizadeh, R. (2013). Laponite clay as a carrier for in situ delivery of tetracycline. *RSC Advances, 3*, 20193–20201.

Green, B. (2004). Focus on aripiprazole. *Current Medical Research Opinion, 20*, 207–213.

Hamilton, A.R., Hutcheon, G.A., Roberts, M., & Gaskell, E.E., (2014). Formulation and antibacterial profiles of clay-ciprofloxacin composites. *Applied Clay Science, 87*, 129–135.

Han, H.K., Lee, Y.C., Lee, M.Y., Patil, A.J., & Shin, H.J. (2011). Magnesium and calcium organophyllosilicates: synthesis and in vitro cytotoxicity study. *ACS Applied Materials & Interfaces, 3*, 2564–2572.

Harrison, T.S. and Perry, C.M. (2004). Aripiprazole: a review of its use in schizophrenia and schizoaffective disorder. *Drugs, 64*, 1715–1736.

Iliescu, R.I., Andronescu, E., Ghitulica, C.D., Voicu, G., Ficai, A., & Hoteteu, M. (2014). Montmorillonite-alginate nanocomposite as a drug delivery system-incorporation and in vitro release of irinotecan. *International Journal of Pharmaceutics, 463*, 184–192.

James L., Groen, S.D., & Coveney, P.V. (2015). Mechanism of exfoliation and prediction of materials properties of clay-polymer nanocomposites from multiscale modeling. *Nano Letters, 15*, 8108–8113.

Joshi, N., Rawatm K., Solanki, P.F., & Bohida, H.B. (2015). Biocompatible laponite ionogels based non-enzymatic oxalic acid sensor. *Sensing and Bio-sensing Research, 5*, 105–111.

Jung, H., Kim, H.M., Choy, Y.B., Hwang, S.J., & Choy, J.H. (2008). Laponite-based nanohybrid for enhanced solubility and controlled release of itraconazole. *International Journal of Pharmaceutics, 349*, 283–290.

Kaassis A.Y.A., Xu, S.M., Guan, S., Evans, D.G., Wei, M., & Williams, G.R. (2016). Hydroxy double salts loaded with bioactive ions: Synthesis, intercalation mechanisms, and functional performance. *Journal of Solid State Chemistry, 238*, 129–138.

Kawase, M., Hayashi, Y., Kinoshita, F., Yamato, E., Miyazaki, J., Yamakawa, J., Ishida, T., Tamura, M., & Yagi, K. (2004). Protective effect of montmorillonite on plasmid DNA in oral gene delivery into small intestine. *Biological and Pharmaceutical Bulletin, 27*, 2049–2051.

Kevadiya, B.D., Thumbar, R.P., Rajput, M.M., Rajkumar, S., Brambhatt, H., Joshi, G.V., Dangi, G.P., Mody, H.M., Gadhia, P.K., & Bajaj, H.C. (2012). Montmorillonite/poly-(ε-caprolactone). composites as versatile layered material: reservoirs for anticancer drug and controlled release property. *European Journal of Pharmaceutical Sciences, 47*, 265–272.

Khalil, M.M., Tremoleda, J.L., Bayomy, T.B., & Gsell, W. (2011). Molecular SPECT imaging: an overview. *International Journal of Molecular Imaging, 2011*, 1–15.

Kim, M.H., Hur, W., Choi, G., Min, H.S., Choy, Y.B., & Choy, J.H. (2016). Theranostic bioabsorbable bone fixation plate with drug-layered double hydroxide nanohybrids. *Advance Healthcare Materials, 5*, 2765–2775.

Kim, T.H., Lee, J.A., Choi, S.J., & Oh, J.M. (2014). Polymer coated CaAl-layered double hydroxide nanomaterials for potential calcium supplement. *International Journal of Molecular Sciences, 15*, 22563–22579.

https://doi.org/10.1007/s42860-019-0009-9 Published online by Cambridge University Press

Kim, T.H., Lee, J.Y., Kim, M.K., Park, J.H., & Oh, J.M. (2016). Radioisotope Co-57 incorporated layered double hydroxide nanoparticles as a cancer imaging agent. *RSC Advances, 6*, 48415–48419.

Kim, J.Y., Yang, J.H., Lee, J.H., Choi, G., Park, D.H., Jo, M.R., Choi, S.J., & Choy, J.H. (2015). 2D inorganic-antimalarial drug-polymer hybrid with pH responsive solubility. *Chemistry - An Asian Journal, 10*, 2264–2271.

Lee, J.H., Choi, G., Oh, Y.J., Park, J.W., Choy, Y.B., Park, M.C., Yoon, Y.J., Lee, H.J., Chang, H.C., & Choy, J.H. (2012). A nanohybrid system for taste masking of sildenafil. *International Journal of Nanomedicine, 7*, 1635–1649.

Lee, J.E., Gwak, G.H., Cho, H.M., Kim, C.Ch., Lee, M.E., & Oh, J.M. (2016). Controlled drug release in silicone adhesive utilizing particulate additives. *Korean Journal of Chemical Engineering, 34*, 1600–1603.

Long, M., Zhang, Y., Huang, P., Chang, S., Hu, Y., Yang, Q., Mao, L., & Yang, H. (2018). Emerging nanoclay composite for effective hemostasis. *Advanced Functional Materials, 28*, 1704452–1704461.

Lvov, Y.M., Devilliers, M.M., & Fakhrullin, R.F. (2016). The application of halloysite tubule nanoclay in drug delivery. *Expert Opinion on Drug Delivery, 13*, 977–986.

Ma, R., Liu, Z., Li, L., Lyi, N., & Sasaki, T. (2006). Exfoliating layered double hydroxides in formamide: a method to obtain positively charged nanosheets. *Journal of Materials Chemistry, 16*, 3809–3813.

Maisanaba, S., Pichardo, S., Puerto, M., Gutiérrez-Praena, D., Cameán, A.M., & Jos, A. (2015). Toxicological evaluation of clay minerals and derived nanocomposites: a review. *Environmental Research, 138*, 233–254.

Margarita, D., López-Blanco, M., Aranda, P., Leroux, F., & Ruiz-Hitzky, E. (2005). Bio-nanocomposites based on layered double hydroxides. *Chemistry of Materials, 17*, 1969–1977.

Marwah, H., Garg, T., Goyal, A.K., & Rath, G. (2016). Permeation enhancer strategies in transdermal drug delivery. *Drug Delivery, 23*, 564–578.

Massaro, M., Colletti, C.G., Noto, R., Riela, S., Poma, P., Guernelli, S., Parisi, F., Milioto, S., & Lazzara, G. (2015). Pharmaceutical properties of supramolecular assembly of co-loaded cardanol/triazole-halloysite systems. *International Journal of Pharmaceutics, 478*, 476–485.

McRobbie, D.W., Moore, E.A., & Graves, M.J. (2017). MRI from Picture to Proton. *Cambridge University Press*, pp. 1–7.

Mosmann, T. (1983). Rapid colorimetric assay for cellular growth and survival: application to proliferation and cytotoxicity assays. *Journal of Immunological Methods, 65*, 55–63.

Mustafa, R., Hu, Y., Yang, J., Chen, J., Wang, H., Zhang, G., & Shi, X. (2016). Synthesis of diatrizoic acid-modified LAPONITE® nanodisks for CT imaging applications. *RSC Advances, 6*, 57490–57496.

Nair, B.P., Sindhu, M., & Nair, P.D. (2016). Polycaprolactone-laponite composite scaffold releasing strontium ranelate for bone tissue engineering applications. *Colloids and Surfaces B, 143*, 423–430.

Oh, J.M., Biswick, T.T., & Choy, J.H. (2009). Layered nanomaterials for green materials. *Journal of Materials Chemistry, 19*, 2553.

Oh, Y.J., Choi, G., Choy, Y.B., Park, J.W., Park, J.H., Lee, H.J., Yoon, Y.J., Chang, H.C., & Choy, J.H. (2013). Aripiprazole-montmorillonite: a new organic-inorganic nanohybrid material for biomedical applications. *Chemistry - A European Journal, 19*, 4869–4875.

Oh, J.M., Choi, S.J., Kim, S.T., & Choy, J.H. (2006). Cellular uptake mechanism of an inorganic nanovehicle and its drug conjugates: enhanced efficacy due to clathrin-mediated endocytosis. *Bioconjugate Chemistry, 17*, 1411–1417.

Oh, J.M., Choi, S.J., Lee, G. E., Kim, J.E., & Choy, J.H. (2009). Inorganic metal hydroxide nanoparticles for targeted cellular uptake through clathrin-mediated endocytosis. *Chemistry - An Asian Journal, 4*, 67–73.

Park, D.H., Cho, J., Kwon, O.J. Yun, C.O., & Choy, J.H. (2016). Biodegradable inorganic nanovector: passive versus active tumor targeting in siRNA transportation. *Angewandte Chemie International Edition, 55*, 4582–4586.

Park, J.K., Choy, Y.B., Oh, J.M., Kim, J.Y., Hwang, S.J., & Choy, J.H. (2008). Controlled release of donepezil intercalated in smectite clays. *International Journal of Pharmaceutics, 539*, 198–204.

Park, D.H., Hwang, S.J., Oh, J.M., Yang, J.H., Choy, J.H. (2013). Polymer−inorganic supramolecular nanohybrids for red, white, green, and blue applications. *Progress in Polymer Science, 38*, 1442–1486.

Prausnitz, M.R., & Langer, R. (2008). Transdermal drug delivery. *Nature Biotechnology, 26*, 1261–1268.

Ray, S., Saha, S., Sa, B., & Chakraborty, J. (2017). In vivo pharmacological evaluation and efficacy study of methotrexate-encapsulated polymer-coated layered double hydroxide nanoparticles for possible application in the treatment of osteosarcoma. *Drug Delivery and Translational Research, 7*, 259–275.

Reichle, W.T. (1986). Synthesis of anionic clay minerals (mixed metal hydroxides, hydrotalcite). *Solid State Ionics, 22*, 135–141.

Ryu, S.J., Jung, H., Oh, J.M., Lee, J.k., & Choy, J.H. (2010). Layered double hydroxide as novel antibacterial drug delivery system. *Journal of Physics and Chemistry of Solids, 71*, 685–688.

Saha, K., Butola, B.S., & Joshi, M. (2014). Synthesis and characterization of chlorhexidine acetate drug-montmorillonite intercalates for antibacterial applications. *Applied Clay Science, 101*, 477–483.

Sarcinelli, M.A., de Souza Albernaz, M., Szwed, M., Iscaife, A., Leite, K.R.M., Junqueira, M., Bernardes, E.S., Silva, E.O., Tavares, M.I.B., & Santos-Oliveira, R. (2016). Nanoradiopharmaceuticals for breast cancer imaging: development, characterization, and imaging in inducted animals. *OncoTargets and Therapy, 9*, 5847–5854.

Shi, S., Fliss, B.C., Gu, Z., Zhu, Y., Hong, H., Valdovinos, H.F., Hernandez, R., Goel, S., Luo, H., Chen, F., Barnhart, T.E., Nickles, R.J., & Xu, Z.P. (2015). Chelator-free labeling of layered double hydroxide nanoparticles for in vivo PET imaging. *Scientific Reports, 5*, 16930.

Soussou, A., Gammoudi, I., Kalboussi, A., Grayby-Heywang, C., Cohen-Bouhacina, T., & Baccar, Z.M. (2017). Hydrocalumite thin films for polyphenol biosensor elaboration. *IEEE Transacions on NanoBioscience, 16*, 650–655.

Stephen, Z.R., Kievit, F.M., & Zhang, M. (2011). Magnetite nanoparticles for medical MR imaging. *Materials Today, 14*, 330–338.

Stockert, J.C., Blázquez-Castro, A., Cañete, M., Horobin, R.W., & Villanueva, Á. (2012). MTT assay for cell viability: Intracellular localization of the formazan product is in lipid droplets. *Acta Histochemica, 114*, 785–796.

Suh, Y.J., Kil, D.S., Chung, K.S., Abdullayev, E., Lvov, Y.M., & Mongayt, D. (2011). Natural nanocontainer for the controlled delivery of glycerol as a moisturizing agent. *Journal of Nanoscience and Nanotechnology, 11*, 611–665.

Thakur, G., Singh, A., & Singh, I. (2016). Formulation and evaluation of transdermal composite films of chitosan-montmorillonite for the delivery of curcumin. *International Journal of Pharmaceutical Investigation, 6*, 23–31.

Vergaro, V., Abdullayev, E., Lvov, Y.M., Zeitoun, A., Cingolani, R., Rinaldi, R., & Leporatti, S. (2010). Cytocompatibility and uptake of halloysite clay nanotubes. *Biomacromolecules, 11*, 820–826.

Vergaro, V., Lvov, Y.M., & Leporatti, S., (2012). Halloysite clay nanotubes for resveratrol delivery to cancer cells. *Macromolecular Bioscience, 12*, 1265–1271.

Wang, X., Gong, J., Rong, R., Gui, Z., Hu, T., & Xu, X. (2018). Halloysite nanotubes-induced Al accumulation and fibrotic response in lung of mice after 30-day repeated oral administration. *Journal of Agricultural and Food Chemistry, 66*, 2925–2933.

Wang, G., Maciel, D., Wu, Y., Rodrigues, J., Shi, X., Yuan, Y., Liu, C., Tomas, H., & Li, Y. (2014). Amphiphilic polymer-mediated formation of laponite-based nanohybrids with robust stability and pH sensitivity for anticancer drug delivery. *ACS Applied Materials & Interfaces, 6*, 16687–16695.

https://doi.org/10.1007/s42860-019-0009-9 Published online by Cambridge University Press

Wang, C., Wang, S., Li, K., Li, J., Zhang, Y., Li, J., Liu, X., Shi, X., & Zhao, Q. (2014). Preparation of laponite bioceramics for potential bone tissue engineering applications. *PLOS One, 9*, e99585

Wang, L., Xing, H., Zhang, S., Ren, Q., Pan, L., Zhang, K., Bu, W., Zheng, X., Zhou, L., Peng, W., Hua, Y., & Shi, J. (2013). A Gd-doped Mg-Al-LDH/Au nanocomposite for CT/MR bimodal imagings and simultaneous drug delivery. *Biomaterials, 34*, 3390–3401.

Wei, W., Minullina, R., Abdullayev, E., Fakhrullin, R., Mills, D., & Lvov, Y. (2014). Enhanced efficiency of antiseptics with sustained release from clay nanotubes. *RSC Advances, 4*, 488–494.

Wen, X., Yang, Z., Yan, J., & Xie, X. (2015). Green preparation and characterization of a novel heat stabilizer for poly(vinyl chloride)-hydrocalumites. *RSC Advances, 5*, 32020–32026

Wu, Y.P., Yang, J., Gao, H.Y., Shen, Y., Jiang, L., Zhou, C., Li, Y.F., He, R.R., & Liu, M. (2018). Folate-conjugated halloysite nanotubes, an efficient drug carrier, deliver doxorubicin for targeted therapy of breast cancer. *ACS Applied Nano Matererials, 1*, 595–608.

Xavier, J.R., Thakur, T., Desai, P., Jaiswal, M.K., Sears, N., Cosgriff-Hernandez, E., Kaunas, R., & Gaharwar, A.K. (2015). Bioactive nanoengineered hydrogels for bone tissue engineering: a growth-factor-free approach. *ACS Nano, 9*, 3109–3118.

Xing, H., Hwang, K., & Lu, Y. (2016). Recent developments of liposomes as nanocarriers for theranostic applications. *Theranostics, 6*, 1336–1352.

Yah, W.O., Takahara, A., Lvov, Y.M. (2012). Selective modification of halloysite lumen with octadecylphosphonic acid: new inorganic tubular micelle. *Journal of the American Chemical Society, 134*, 1853–1859.

Yang, J.H., Han, Y.S., Park, M., Park, T., Hwang, S.J., & Choy, J.H. (2007). New Inorganic-based drug delivery system of indole-3-acetic acid-layered metal hydroxide nanohybrids with controlled release rate. *Chemistry of Materials, 19*, 2679–2685.

Yang, J.H., Jung, H., Kim, S.Y., Yo, C.H., & Choy, J.H. (2013). Heterostructured layered aluminosilicate-itraconazole nanohybrid for drug delivery system. *Journal of Nanoscience and Nanotechnology, 13*, 7331–7336.

Yang, L., Shao, Y., & Han, H.K. (2014). Improved pH-dependent drug release and oral exposure of telmisartan, a poorly soluble drug through the formation of drug-aminoclay complex. *International Journal of Pharmaceutics, 471*, 258–263.

Yuan, P., Tan, D., & Annabi-Bergaya, F. (2015). Properties and applications of halloysite nanotubes: recent research advances and future prospects. *Applied Clay Science, 112-113,* 75–93.

Zhou, T., Jia, L., Luo, Y.F., Xu, J., Chen, R.H., Ge, Z.J., Ma, T.L., Chem, H., & Zhu, T.F. (2016). Multifunctional nanocomposite based on halloysite nanotubes for efficient luminescent bioimaging and magnetic resonance imaging. *International Journal of Nanomedicine, 11*, 4765–4776.

Zhuang, Y., Zhao, L., Zheng, L., Hu, Y., Ding, L., Liu, C., Zhao, J., Shi, X., & Guo, R. (2017). LAPONITE-polyethylenimine based theranostic nanoplatform for tumor-targeting CT imaging and chemotherapy. *ACS Biomaterials Science & Engineering, 3*, 431–442.

[*Received 28 April 2018; revised 23 August 2018; AE: J.W. Stucki*]

https://doi.org/10.1007/s42860-019-0009-9 Published online by Cambridge University Press